Predictive modelling of L and H confinement modes and edge pedestal characteristics

D. Kalupin[1]**, M.Z. Tokar**[1]**, B. Unterberg**[1]**, X. Loozen**[1] **and D. Pilipenko**[2]

[1] Institut für Plasmaphysik, Forschungszentrum Jülich GmbH, EURATOM Association,
D-52425 Jülich, Germany
[2] Université Libre de Bruxelles, CP 231, Bvd du Triomphe, Association EURATOM-Etat
Belge, B-1050 Bruxelles, Belgium

E-mail: d.kalupin@fz-juelich.de

Abstract
The results of predictive self-consistent modelling of plasma parameters in low (L) and high (H) confinement modes by the one-dimensional transport code RITM, with particular emphasis on the properties of the edge transport barrier, are presented and discussed. The same transport model is used under both L- and H-mode conditions and includes contributions from ion temperature gradient (ITG), trapped electron, drift Alfvén (DA) and drift resistive ballooning instabilities described in the fluid approximation. The computations predict the formation of the edge transport barrier at a high enough heating power due to stabilization of ITG and DA modes, dominating the edge transport in the L-mode, through the effects of the density gradient and the pressure gradient at low collisionality, respectively. The calculated radial profiles and scalings for pedestal and confinement characteristics are compared with measurements on JET, DIII-D and JT-60U tokamaks.

PACS numbers: 52.35.Py, 52.55.Fa

1. Introduction

The shear of the radial electric field is generally considered as the main cause of confinement improvement in fusion plasmas under the H-mode conditions [1, 2]. However, by applying this postulate to a particular situation, one has to take into account the specific nature of transport mechanisms, whose suppression leads to the improvement. Diverse approaches have been proposed in order to explain the transport in fusion plasmas. Different types of micro-instabilities were discussed as dominating anomalous transport processes in the plasma core and at the edge, as well as different methods to model these instabilities, i.e. fluid, gyro-kinetic, linear, non-linear, etc, were considered. The main purpose of this study is a self-consistent computation of the plasma profiles over the whole plasma radius including the edge transport barrier. This is a difficult problem by itself because (i) transport coefficients undergo a strong change at the interface between the core and barrier regions and (ii) the interface position is not known *a priori*. Therefore, as the first approximation, a relatively reduced transport model based on a fluid approximation is used. This, nonetheless, includes contributions from the most

important unstable modes and describes a strong reduction of the edge transport under the H-mode conditions. In spite of the models 'simplicity', the resulting transport coefficients depend extremely non-linearly on the plasma parameters and their gradients imposing serious requirements on the code applied for solving the transport equations.

In the case of the edge transport barrier, instabilities of a different nature should be taken into consideration [3]. Specific 'edge' instabilities, drift Alfvén (DA) and drift resistive ballooning (DRB) modes, are triggered by Coulomb collisions and, therefore, are of importance only at a relatively low temperature. Numerical modelling of edge turbulence [4] predicts that the $\boldsymbol{E} \times \boldsymbol{B}$ rotation shear alone is not capable of stabilizing these modes and low plasma collisionality in combination with high pressure gradient is required. An analytical model for DA turbulence, which takes these mechanisms into account, has been developed in [5]. It predicts that this channel of particle and energy losses, controlling the edge transport under L-mode conditions, becomes drastically reduced if the heating power exceeds a critical value. Predictive modelling of radial profiles in H-mode plasmas performed in [6]

by using this model, has revealed good agreement with experimental data.

An analysis of results in [5] shows that the dominance of the temperature gradient in the pressure gradient plays an important role in the reduction of DA transport. The same effect is of significance for the stabilization of collisionless universal drift waves (DWs) [7]. In the present consideration, DWs are not taken into account since they are damped in a linear approximation by a magnetic shear [8]. When non-linear dynamics is involved DW becomes self-sustaining [9], but the induced transport is significantly reduced by an increasing temperature gradient [10]. Therefore, we expect that the present approach provides qualitatively correct results even without DW contribution to the transport. Nevertheless, in order to enhance the reliability of results, the calculation of plasma parameter profiles should be integrated in future with a consistent non-linear modelling of particle and energy transport.

The suppression of edge turbulence is necessary but not enough for the formation of the H-mode pedestal. Additionally, the modes dominating transport in the plasma core should be damped in the barrier region. Thus, the current diffusive ballooning mode (CDBM) [11] is strongly reduced by the magnetic shear. Our computations show that under the conditions of H-mode without internal transport barriers, CDBM induced transport plays, in the outer half of the plasma minor radius, a much smaller role than ion temperature gradient (ITG) and trapped electron (TE) unstable modes [13]. ITG instability can be effectively stabilized by the density gradient, since the latter essentially determines the critical temperature gradient [13, 14]. Especially at the plasma edge, where the density gradient is the largest due to the ionization of neutrals penetrating into the confined volume through the separatrix, it crucially assists the shear of $E \times B$ rotation in the suppression of ITG transport. Moreover, the present calculations demonstrate that only when the effect of the density gradient is taken into account, can important experimentally observed features of the L–H transition and characteristics of the edge transport barrier be explained. For the suppression of dissipative TE modes in the barrier the low plasma collisionality plays an important role [15, 16].

2. Code RITM

2.1. Transport equations

The numerical modelling of L- and H-mode plasmas in JET is done by using the one-dimensional transport code RITM [17–22]. This code allows us to compute the variation of diverse plasma parameters with time and the effective minor radius of the magnetic surface, r, in the confined plasma region from the plasma axis to the separatrix. Neutrals produced by plasma recycling on divertor plates and entering the confined volume through the separatrix are described by the velocity distribution function f_n. This is governed by the kinetic equation:

$$\frac{1}{g_1} \frac{\partial}{\partial r}(v_r f_n) = S_n - \nu_n f_n, \qquad (1)$$

where v_r, S_n and ν_n are the radial velocity, source density and ionization frequency of neutral particles, respectively.

By applying a diffusive approximation [23], equation (1) is reduced to equations for the neutral particle and flux densities.

The densities of electrons and impurity ions, n_e, and n_Z, respectively, are determined from continuity equations:

$$\frac{\partial n_e}{\partial t} + \frac{1}{rg_1} \frac{\partial}{\partial r}(rg_2 \Gamma_\perp^e) = S_n + \sum_Z Z S_Z, \qquad (2)$$

$$\frac{\partial n_Z}{\partial t} + \frac{1}{rg_1} \frac{\partial}{\partial r}(rg_2 \Gamma_\perp^Z) = S_Z, \qquad (3)$$

where $S_{n,Z}$ are the densities of charged particle sources due to ionization, recombination and charge-exchange of impurity ions with the main neutrals; ions of all charges Z of He, C, O, Ne, Si and Ar impurities can be taken into account in the calculation. The radial distribution of the particle source due to neutral beam injection is taken from the experimental data [22, 24].

The densities of particle fluxes include both diffusive and convective contributions:

$$\Gamma_\perp^e = -D_\perp^e \frac{\partial n_e}{\partial r} + V_\perp^e n_e, \qquad \Gamma_\perp^Z = -D_\perp^Z \frac{\partial n_Z}{\partial r} + V_\perp^Z n_Z. \qquad (4)$$

The densities and fluxes of the background ions are computed from the quasi-neutrality conditions:

$$n_i = n_e - \sum Z \cdot n_Z, \qquad \Gamma_\perp^i = \Gamma_\perp^e - \sum Z \cdot \Gamma_\perp^Z. \qquad (5)$$

The metric coefficients $g_{1,2}$, characterizing the magnetic equilibrium, are determined by using the Shafranov shift, calculated from the Grad–Shafranov equation, and analytically prescribed elongation δ and triangularity κ of the magnetic surfaces.

The electron and ion temperatures, T_e and T_i, are determined from the heat transport equations:

$$\frac{3}{2} \frac{\partial n_e T_e}{\partial t} + \frac{1}{rg_1} \frac{\partial}{\partial r}\left[rg_2\left(1.5\,\Gamma_\perp^e T_e - \kappa_\perp^e \frac{\partial T_e}{\partial r}\right)\right]$$
$$= Q_{oh} + Q_{au}^e - Q_{ei} - Q_{en} - Q_{eI}, \qquad (6)$$

$$\frac{3}{2} \frac{\partial n_\Sigma T_i}{\partial t} + \frac{1}{rg_1} \frac{\partial}{\partial r}\left[rg_2\left(1.5\,\Gamma_\perp^\Sigma T_i - \kappa_\perp^\Sigma \frac{\partial T_i}{\partial r}\right)\right]$$
$$= Q_{au}^i + Q_{ei} + Q_{in}, \qquad (7)$$

where $n_\Sigma = n_i + \Sigma n_Z$, $\Gamma_\Sigma = \Gamma_i + \Sigma \Gamma_Z$ and Q_{oh} and $Q_{au}^{e,i}$ are the densities of heating sources due to Ohmic dissipation and additional heating from neutral beams and radio-frequency waves, respectively; the radial profile of $Q_{au}^{e,i}$ is taken from experiment [22, 24]; Q_{ei}, Q_{en}, Q_{eI} are the energy losses from electrons due to Coulomb collisions with ions, excitation and ionization of neutrals and impurities, respectively, and Q_{in} the energy exchange between main ions and neutrals by ionization and charge-exchange.

The boundary conditions of equations (2), (3), (6) and (7) at the separatrix, $r = a$, imply the e-folding lengths of parameters, which are taken from measurements.

2.2. Transport model

2.2.1. Linearized equations for small perturbations. The transport model in RITM accounts for the most important unstable drift modes. These are divided into two groups of

'core' and 'edge' instabilities treated separately by using two-fluid MHD equations linearized for small perturbations of plasma parameters proportional to $\exp(-i\omega t + iky)$. Here, ω is the complex frequency and k the wave vector component in the direction y on the magnetic surface perpendicular to the field lines.

The first 'core' group includes ITG–TE modes, which are described by taking into account the perturbations of density, ion temperature and electric potential, $\tilde{n}$, $\tilde{T}_i$ and $\tilde{\varphi}$, respectively. They are governed by the linearized ion and electron continuity equations [13, 25]:

$$-i\omega\tilde{n} + \tilde{V}_{i,r}\frac{dn}{dr} = 0, \tag{8}$$

$$\tilde{n} = \left(1 + f_{tr}\frac{\omega_* - \omega + i\nu_{eff}(\omega_{Te}/(\omega - \omega_D + i\nu_{eff}))}{\omega + i\nu_{eff}}\right)\frac{en\tilde{\varphi}}{T_e} \tag{9}$$

and the ion heat balance equation:

$$\left(\omega_{Ti} - \frac{2}{3}\omega_*\right)\frac{e\tilde{\varphi}}{T_e} + \frac{2}{3}\omega\frac{\tilde{n}}{n} = \left(\omega + \frac{5}{3}\tau\omega_D\right)\frac{\tilde{T}_i}{T_i}. \tag{10}$$

Here $\tilde{V}_{i,r}$ is the perturbed radial ion velocity, which includes $\boldsymbol{E}\times\boldsymbol{B}$, polarization, diamagnetic and gyro–viscous drift contributions, f_{tr} the fraction of trapped particles,

$$\omega_* = \frac{cT_ek}{eB}\left(-\frac{d\ln n_e}{dr}\right), \qquad \omega_{Te,i} = \frac{cT_ek}{eB}\left(-\frac{d\ln T_{e,i}}{dr}\right),$$

$$\omega_D = \frac{2cT_ek}{eBR}$$

are characteristic drift frequencies, $\nu_{eff} = \nu_{ei}R/r$ the effective collision frequency of TEs with ν_{ei} being the collision frequency of thermal electrons, c the speed of light, e the elementary charge, B the magnetic field induction, $\tau = T_i/(Z_{eff}T_e)$ and Z_{eff} is the ion effective charge.

For the 'edge' DA–DRB modes, the perturbation of electric current is of importance. Its perpendicular components, $\tilde{j}_r$ and $\tilde{j}_y$, are determined from the corresponding components of the momentum equation for ions:

$$-i\omega m_i n\tilde{V}_{i,r} = \frac{\tilde{j}_y B}{c}, \qquad ik(T_e + T_i)\tilde{n} = -\frac{\tilde{j}_r B}{c}. \tag{11}$$

The parallel component, $\tilde{j}_\parallel$, is governed by the charge conservation condition:

$$\vec{\nabla}\cdot\vec{j} = \frac{\partial\tilde{j}_\parallel}{\partial l} + ik_y\tilde{j}_y + \frac{\partial\tilde{j}_r}{\partial r} = 0. \tag{12}$$

It is assumed that only electron parallel motion is of importance, i.e. $\tilde{j}_\parallel = -en\tilde{V}_{e,\parallel}$, and the perturbation $\tilde{V}_{e,\parallel}$ of the electron parallel velocity is determined by the parallel momentum balance equation, i.e. Ohm's law:

$$-i\omega m_e\tilde{V}_{e,\parallel} = -en\tilde{E}_\parallel - T_e\nabla_\parallel\tilde{n} - \frac{\partial(nT_e)}{\partial r}\frac{\tilde{B}_r}{B_0} + m_e\nu_{ei}\frac{\tilde{j}_\parallel}{e}. \tag{13}$$

Perturbations of the parallel electric field and radial magnetic field are given by Maxwell's equations:

$$\tilde{E}_\parallel = i\frac{4\pi\omega}{k_y^2 c^2}\tilde{j}_\parallel - \nabla_\parallel\tilde{\varphi}, \qquad \tilde{B}_r = i\frac{4\pi}{k_y^c}\tilde{j}_\parallel. \tag{14}$$

By combining equations (8)–(10) one gets a dispersion relation between ω and k for 'core' modes. In the case of 'edge' instabilities, equations (8), (11)–(14) result in an eigenfunction equation of the Mathieu type describing the variation of the electric potential perturbation amplitude with the poloidal angle [26]. The dispersion relation in this case follows from the properties of Mathieu functions. In order to find ω as a function of k and other parameters, the obtained dispersion equations are solved by using standard subroutines.

2.2.2. Transport coefficients. The transport coefficients are evaluated by taking into account only the perturbations with the maximum growth rate $\gamma = \text{Im}\omega$ as a function of the wave number k. The particle flux, generated by the radial drift due to the perturbed poloidal electric field with the velocity $V_E = ikc\tilde{\varphi}/B$, is given by the relation [13]:

$$\Gamma_e = \tilde{n}V_E^* + \tilde{n}^*V_E = \frac{2c(\text{Re}\,\tilde{n}\,\text{Im}\,\tilde{\varphi} - \text{Im}\,\tilde{n}\,\text{Re}\,\tilde{\varphi})\,k_y}{B}.$$

The density and potential perturbations here are linked through equation (8). On a non-linear stage the $\tilde{\varphi}$ amplitude is saturated at a level where the perturbation drive due to linear instability is counterbalanced by the outflow due to $\boldsymbol{E}\times\boldsymbol{B}$ convection: $\gamma\tilde{n}\sim V_E\nabla\tilde{n}$. As a result, one gets a quasi-linear approximation [13]: $e\phi/T_e \approx \gamma/(\omega_{*e}k_xL_n)$. Finally, the anomalous diffusivity D is determined from the definition: $\Gamma_e = -D\nabla n$. By neglecting finite Larmor radius effects, this procedure leads to the prominent improved mixing length approximation [13],

$$D \approx \frac{\gamma}{k^2}\frac{\gamma^2}{\gamma^2 + \omega_r^2},$$

where ω_r is the real frequency of perturbations.

Numerical modelling of radial profiles with the transport model described above is very time consuming. In order to avoid this, approximate solutions of dispersion equations can be used to estimate the frequencies, growth rates and wave numbers of individual unstable modes. In such an approximation the contributions to anomalous transport from ITG and TE are given by the relations [13, 15]

$$D^{ITG} \approx \frac{cT_e}{k_{ITG}eB}\left[\left(-\frac{d\ln T_i}{dr} + \frac{2}{3}\frac{d\ln n_e}{dr}\right)\frac{\tau}{R(1 - f_{tr})} - \frac{1}{8}\left(\frac{d\ln n_e}{dr} + \frac{2}{R}\right)^2\frac{1}{(1 - f_{tr})^2} - \frac{20}{9}\frac{\tau^2}{R^2}\right]^{1/2}, \tag{15}$$

$$D^{TE} \approx \frac{f_{tr}\eta_e}{k_{TE}^2}\frac{\omega_*^2\nu_{eff}}{\omega_*^2 + \nu_{eff}^2}, \tag{16}$$

where $k_{ITG} \approx 0.3/\rho_s$ and $k_{TE} \approx 1/\rho_s$ (ρ_s being the ion Larmor radius) are the k-values at which the maximum growth rates of ITG and TE modes, respectively, are approached and R is the plasma major radius.

Characteristic transport coefficients due to DA and DRB modes were found in [5, 27]:

$$D^{DA} = \frac{\chi_{GB}}{\sqrt{\mu}}\bar{\bar{\chi}}_\perp(\beta_n, \nu_n), \tag{17}$$

$$D^{DRB} = (2q\rho_e)^2\nu_e R\left(-\frac{d\ln n_e}{dr}\right). \tag{18}$$

Here $\chi_{GB} = \rho_s^2 c_s / L_p$ is the Gyro–Bohm diffusion with c_s being the ion sound velocity and $L_p = -dr/d\ln(nT_e)$ the e-folding length for the electron pressure; $\mu = -k_\parallel L_p \sqrt{m_i T_e/(m_e T_i)}$ with $k_\parallel \sim 1/qR$; the factor

$$\bar{\bar{\chi}}_\perp(\beta_n, \nu_n) = \left[\frac{(1+\beta_n^2)^{-3} + \nu_n^2}{1+\beta_n^2 + \nu_n^{4/3}} \right]^{1/2}$$

depends on parameters

$$\beta_n = \left(\frac{m_i}{m_e}\right)^{1/2} \frac{\beta}{k_\parallel L_p}$$

and

$$\nu_n = \left(\frac{m_i}{m_e}\right)^{1/4} \frac{L_p^{1/2}}{\lambda_e k_\parallel^{1/2}}$$

with $\beta = 4\pi n_e T_e/B^2$ and λ_e being the mean free path length; q is the safety factor and ρ_e the electron Larmor radius.

Combining the contributions from all modes, the effective transport coefficients are assumed in the form

$$D_\perp^e = D^{ITG} f_{tr} + D^{DTE} + D^{DRB} + D^{DA} + D^{CDBM}, \quad (19)$$

$$V_\perp^e = \left[D^{ITG} f_{tr} \left(\frac{4r}{3R}\right) + D^{DTE} + D^{CDBM} \right] \left(\frac{d\ln q}{dr}\right), \quad (20)$$

$$D_\perp^Z = D_\perp^e, \quad (21)$$

$$V_\perp^Z = V_\perp^e + V_\perp^{Z,NEO}, \quad (22)$$

$$\kappa_\perp^e = \tfrac{3}{2}(D^{ITG} f_{tr} + D^{DTE} + D^{DRB} + D^{DA} + D^{CDBM})n_e, \quad (23)$$

$$\kappa_\perp^i = \kappa_\perp^{i,NEO} + \tfrac{3}{2}(D^{ITG} + D^{DRB} + D^{DA} + D^{CDBM})n_\Sigma, \quad (24)$$

where the input from CDBM is estimated according to [11]:

$$D^{CDBM} = \frac{G_0}{1 + G_1 h^2} \alpha^{3/2} \frac{c^2}{\omega_{pe}^2} \frac{\upsilon_A}{qR}, \quad (25)$$

where $G_{0,1}$ are functions of the normalized pressure gradient

$$\alpha = \frac{8\pi R q^2}{B_T^2} \left| \frac{\partial(n_e T_e + n_i T_i)}{\partial r} \right|$$

and the magnetic shear $s = (r/q)(dq/dr)$ given in [12], h is the rotation shear $(qR/\upsilon_A)(1/sB)dE_r/dr$, υ_A is the Alfvén velocity and ω_{pe} is the electron plasma frequency.

The proportionality of the ITG contribution to the particle transport to the fraction of trapped particles, f_{tr}, is explained as follows. In a linear electrostatic approximation ITG instability does not provide particle transport [13]. However, as other drift instabilities on the non-linear turbulent stage, it leads to stochastization of closed drift orbits and generates particle losses. This happens most easily to TEs with low parallel velocity [28]. The small factor $4r/3R$ in the expression for the electron pinch velocity represents a relatively weak effect of ion driven modes on electron convection [29]. The pinch velocity of impurity ions includes, in addition to $V_\perp^e$, the neo-classical contribution $V_\perp^{Z,NEO}$ due to collisions with the background ions [30].

The present version of the code RITM does not permit us to model ELM activity explicitly because, due to non-linear dependence of transport coefficients on the radial gradients of plasma parameters, calculations do not converge reliably for time steps smaller than 5–10 ms. Indirectly, the ELM effect on particle and energy losses is taken into account by increasing
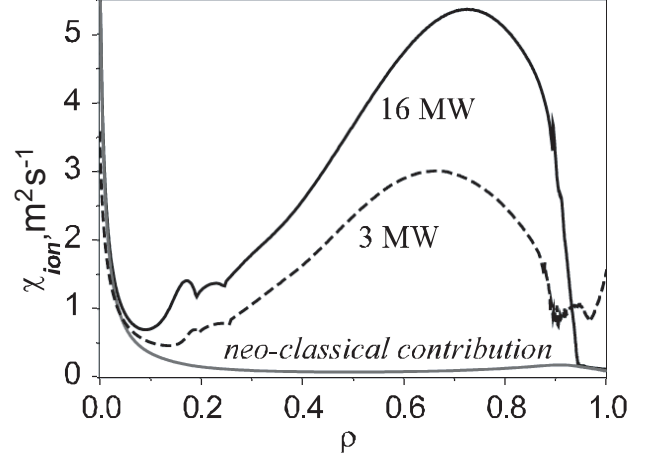

Figure 1. Ion heat diffusion coefficients computed for JET parameters at different levels of additional heating power.

the edge transport as $\exp[(\alpha/\alpha_c)^m]$, with $m \gg 1$, when the normalized pressure gradient α exceeds the ballooning stability limit $\alpha_c = 0.4 s_{95}[1 + \delta_{95}^2(1 + 5\kappa_{95}^2)]$ [31]. Here, s_{95}, δ_{95} and κ_{95} are the values of the magnetic shear, elongation and triangularity at the magnetic surface where the toroidal flux is 95% of its value at the separatrix. According to [31], $\delta_{95} = 0.914\delta_{separatrix}$ and $\kappa_{95} = 0.85\kappa_{separatrix}$.

3. Modelling of L- and H-mode conditions

The formation of a transport barrier at the edge by sufficient plasma heating is the main exceptional feature of the H-mode compared to L-mode performance. In order to demonstrate the capability of the transport code to reproduce both L and H confinement modes, calculations were done for JET plasmas with the following parameters: the magnetic field $B_T = 2.4$ T, plasma current $I_P = 2.3$ MA, with a monotonic profile of the safety factor and $q_{95} = 4$, the elongation and triangularity at the separatrix equal 1.6 and 0.45, respectively. Plasmas of a relatively high line-averaged density, $\bar{n} = 0.7$–1×10^{20} m^{-3}, characteristic for the experiments with deliberate impurity seeding into JET [22, 24] have been modelled.

Figure 1 presents the radial profiles of the total ion heat diffusivity computed using the transport model given by equations (8)–(14). For low heating power χ_{ion} is about 1 m^2 s^{-1} at the plasma edge and is determined mostly by the anomalous contribution. With increased heating the turbulent transport becomes completely suppressed in the region $0.93 \leqslant \rho \leqslant 1$ where the total heat diffusion reduces to the neo-classical level. For the following parametric studies, which required many runs of the code, the approximate transport coefficients in equations (15)–(18) have been used instead of the transport model presented by equations (8)–(14). A comparison of both approaches for some selected cases has shown that they lead to principally similar results.

Figure 2 shows the normalized edge pressure gradient, α, and the ion temperature at a position inside the transport barrier, $\rho = 0.95$, computed versus the total heating power, P_{tot}. One can see a very strong (by a factor of 3–3.5) non-linear increase in both characteristics taking place in a relatively narrow power range of 8–12 MW. The latter clearly separates the two
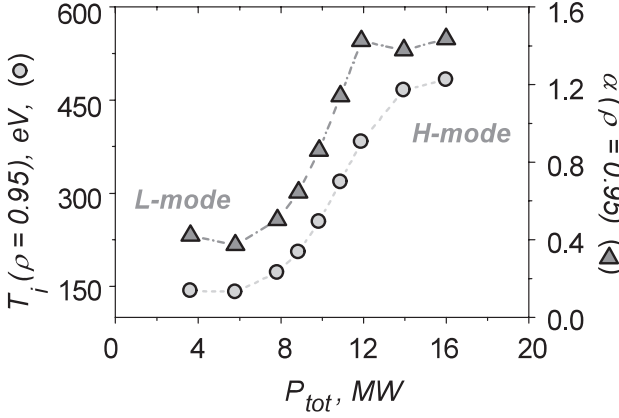
Figure 2. Normalized pressure gradient, α, and ion temperature, T_i, at $\rho = 0.95$ versus the input power.

parameter regions where both α and T_i are weakly dependent on the power. These regions are attributed to L- and H-modes, respectively. Up to now the code RITM does not include a particular physics of the applied auxiliary heating (NBI, ICRH) and its effect on transport. Therefore, an important problem, namely how the heating nature affects the L–H transition, could not be investigated and should be tackled in future studies. The influence of the heating power density profile on the results has been analysed by changing this in two ways: (i) by adding a constant through the radius contribution, which is the same for electrons and ions, to the initial experimental profile for the L-mode conditions, and (ii) by multiplying this profile by a constant factor. It turns out, that the power level at which the L–H transition takes place, is nearly the same in both cases.

Non-linear interrelations between plasma parameters, their gradients and transport characteristics do not permit us to interpret simply and uniquely the mechanism sustaining the reduced edge transport under H-mode conditions. The following one, schematically demonstrated in figure 3, seems to be the most probable. When the heating power increases to the necessary level, the electron temperature grows (figure 3(*a*)), collisionality drops and the pressure gradient rises to a level high enough for a significant reduction of the transport driven by DA instability, equation (17). When this transport channel, being the main one for electrons under L-mode conditions (figure 3(*b*)), is reduced, a steeper density gradient is formed at the edge due to ionization of recycling neutrals (figure 3(*c*)). This allows us to maintain the ITG transport at a low level in spite of increasing ITG (figure 3(*d*)) because, according to equation (15), $D^{ITG} \sim \sqrt{\nabla T - \nabla T_{crit}}$, where the critical temperature gradient ∇T_{crit} increases non-linearly with the density gradient ∇n.

Large temperature and density gradients are considered normally as destabilizing for dissipative TEM [15, 16, 25]. This is, in particular, the case in collisional L-mode plasmas where $\omega_* \ll \nu_{eff}$ and $D^{TE} \sim \eta_e \omega_*^2 / \nu_{eff} \sim \nabla T \nabla n / \nu_{eff}$. However, in the H-mode barrier, $\omega_* \gg \nu_{eff}$ and, according to equation (16), $D^{TE} \sim \eta_e \nu_{eff} \sim \nu_{eff} \nabla T / \nabla n \sim 1/\sqrt{T}$; i.e. TEM induced transport drops with increasing temperature at the edge. Nonetheless, the remaining TEM activity plays an important role by maintaining the steep density gradient at the edge through its contribution to the inward pinch (see equation (20), [14]).

When the major suppliers to the anomalous transport are suppressed, the neo-classical transport provides the dominant contribution to χ_i at the edge (figure 3(*e*)). Formation of the edge transport barrier leads to the pedestal in the temperature and pressure profiles (figures 3(*f*) and (*g*)).

4. Pedestal characteristics

Characteristics of the edge pedestal, e.g. its width and the temperatures at the pedestal top, $T_{i,e}^{Edge}$, are very important for the overall plasma performance [32]. Thus, due to the nature of turbulence triggered by temperature gradients [13, 33], the temperature profiles are stiff in the plasma core and $T_{i,e}^{Edge}$ essentially controls the total plasma thermal energy. The pedestal width, Δ, significantly varies in experiments with different global and local plasma parameters [34, 35]. For the profiles computed by RITM the pedestal width is defined as the distance from the separatrix to the position where a sudden change in the ITG takes place. In order to find the relation between Δ and the line-averaged density, the latter has been changed by RITM calculations through the intensity of deuterium fuelling. The decrease of Δ with density is in good correlation with the observations on DIII-D [34], which were explained by the assumption that Δ is controlled by the penetration depth of neutrals, l_n, being inversely proportional to the plasma density.

Our modelling shows that this dependence is due to the effect of the density gradient on the growth rate of ITG instability. The proportionality between Δ and l_n found in RITM computations, is explicitly demonstrated in figure 4. In addition, the penetration depth of neutrals is proportional to their thermal velocity. After charge-exchange neutrals acquire the ion temperature, one can expect that Δ scales as $\sqrt{T_i^{Edge}}$. Such behaviour, found in experiments on JT-60U [35], is confirmed by the results of our modelling presented in figure 5.

JET plasmas under consideration were characterized by the presence of Type-I ELMs [22, 24]. In computations, the normalized pressure gradient approaches the ideal ballooning stability limit, but does not overcome it. This is due to the strong enhancement of the edge transport assumed in the code when α exceeds α_c.

5. Threshold power for H-mode

The inter-machine analysis [36] provides the scaling for the power threshold of the L–H transition: $P_{th} = 0.042\bar{n}_e^{0.64} B^{0.78} S^{0.94}$, where $\bar{n}_e$ is the line-averaged electron density and S the plasma surface (MW, m^{-3}, T, m^{-2}). The grey area in figure 6 presents the threshold value of $P_{in} - dW/dt$ found in experiments on JET [37], where P_{in} is the total heating power and W is the plasma stored energy. The results of calculations with the code RITM are shown by different symbols.

Because computations do not allow us to resolve a real-time dynamics of the L–H transition, the threshold power is determined in simulations as the power level at which $(d\alpha/dP_{tot})(\rho = 0.95)$ has the maximum slope as a function of P_{tot} (see figure 2). Different symbols for the same toroidal magnetic field were obtained by varying the plasma density
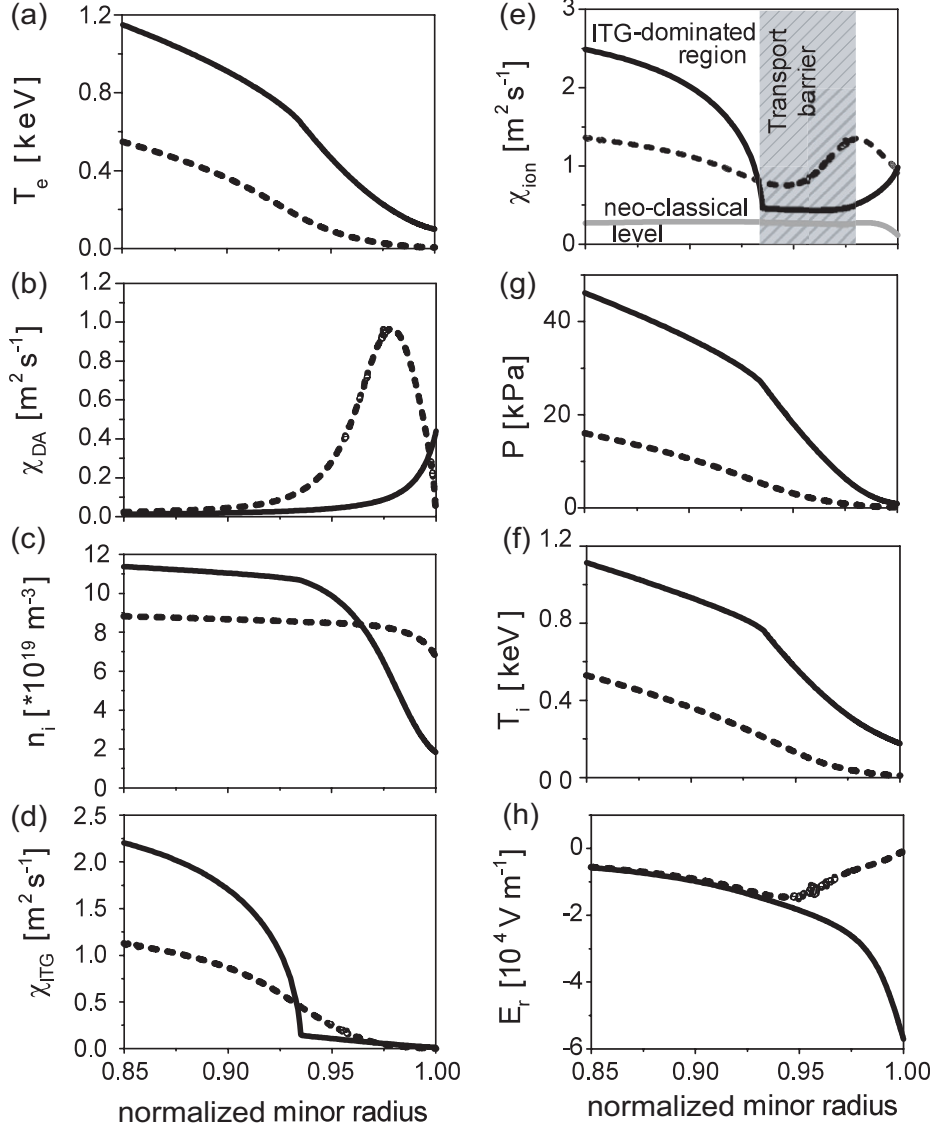
Figure 3. Radial profiles of (*a*) electron temperature, (*b*) heat diffusivity due to DA mode, (*c*) ion density, (*d*) heat diffusivity due to ITG mode, (*e*) total ion heat diffusivity, (*f*) ion temperature, (*g*) total pressure and (*h*) radial electric field, computed for $P_{tot} = 4.2$ MW (- - - -) and $P_{tot} = 14$ MW(——).
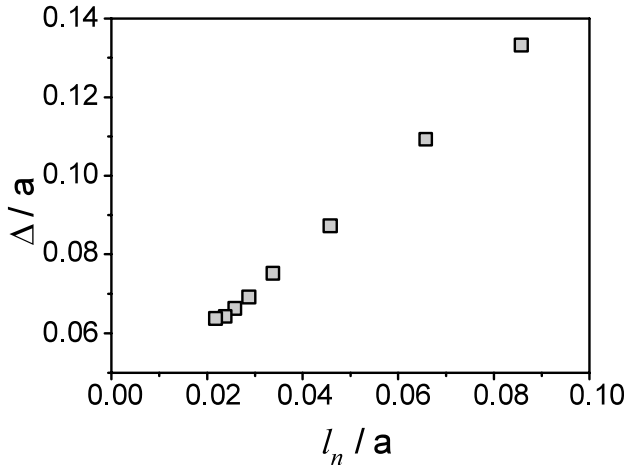

Figure 4. Normalized pedestal width versus normalized penetration depth of recycling neutrals.

at the pedestal top, from 6×10^{19} m^{-3} to 9×10^{19} m^{-3}, for each value of the magnetic field. Although the modelling reproduces the general tendency well, it predicts a density dependence stronger than is given by the scaling law. This can lead to some problems for obtaining the H-mode in future machines like ITER, if the operation is extended to densities noticeably higher than 10^{20} m^{-3}. For nominal ITER parameters, $S = 678$ m^2, $B = 5.3$ T, $n_e = 6 \times 10^{13}$ cm^{-3} [38], our computations predict a power threshold between 30 and 45 MW. According to figure 6, this value can be up to a factor of two larger if the density is increased by 50%.

6. Discussions of the results

6.1. Threshold of L–H transition

The computations above predict a sharp variation of transport coefficients in a narrow range of the power input. However,
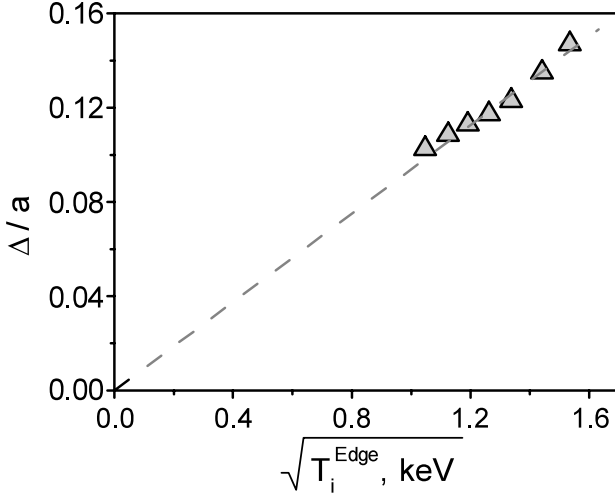
473

Figure 5. Normalized pedestal width as a function of ion temperature at the pedestal top.
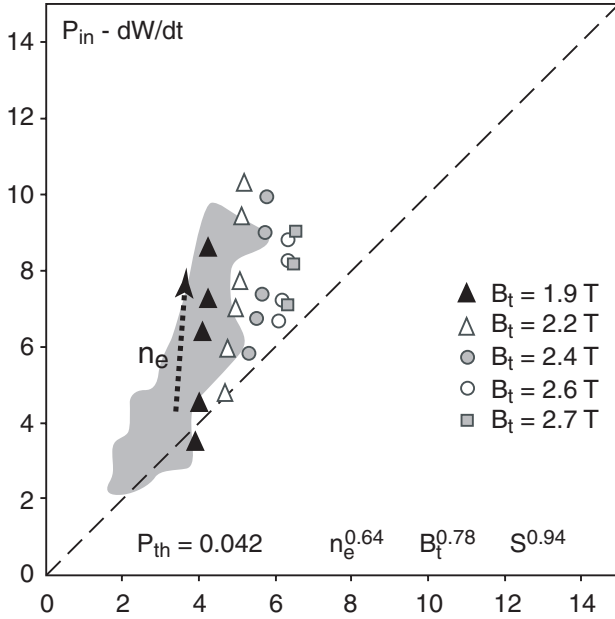

Figure 6. Heating power at the onset of the H-mode in JET from experimental data (grey area) and RITM modelling (symbols) versus the inter-machine scaling [38].

they do not show a bifurcation, contrary to normal belief about the L–H transition. Here, we demonstrate that this is a result of particular conditions considered above, i.e. of high enough density, and that the adopted transport model predicts a bifurcation at a lower density. Consider the heat flux produced by DA modes, $q_\perp = 3D^{DA} n \nabla T + 3D^{DA} \nabla n T = 3D^{DA} \nabla (nT)$. In the parameter ν_n, introduced in [5] and used in equation (17) above, the effects of the collisionality and pressure gradient are mixed. In order to separate them, we make use of the parameter

$$\nu_0 = \frac{\sqrt{\beta}}{\lambda_e k_\parallel} \sqrt{\frac{m_i}{m_e}} \propto \left(\frac{n_e}{T_e}\right)^{3/2},$$
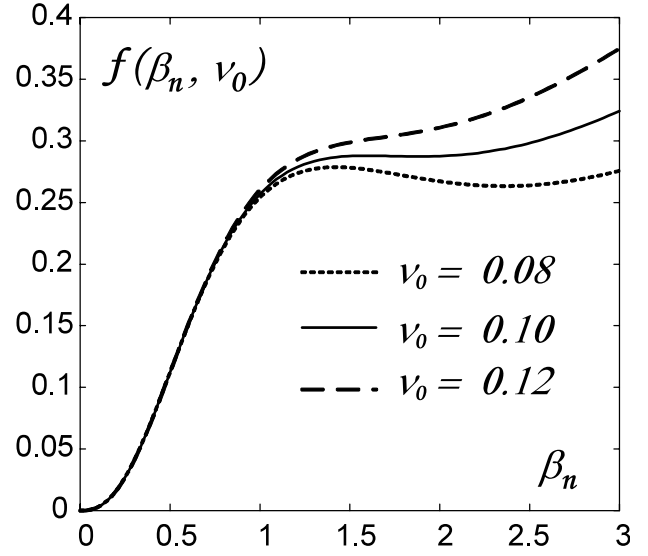

Figure 7. Function $f(\beta_n, \nu_0)$ versus normalized beta for different values of ν_0.

depending on collisionality only. As a result one gets $q_\perp = q_0 f(\beta_n, \nu_0)$, where

$$q_0 = \left(\frac{1}{4\pi}\right)^{5/2} \left(\frac{m_e}{n}\right)^{3/2} \frac{B^3}{m_i} \left(\frac{c}{eqR}\right)^2$$

and

$$f(\beta_n, \nu_0) = \frac{\beta_n^{5/2}}{(1 + \beta_n^2)^{3/2}} \left[\frac{1 + \nu_0^2 (1 + \beta_n^2)^3 / \beta_n}{1 + \beta_n^2 + \nu_0^{4/3} / \beta_n^{2/3}}\right]^{1/2}. \quad (26)$$

The factor $f(\beta_n, \nu_0)$ is shown in figure 7 as a function of β_n for several ν_0. The stationary value of β_n and thus of the pressure gradient at the edge, is determined by the intersection of these curves with the horizontal line q_{core}/q_0, where q_{core} is the density of the heat flux from the core into the edge region. With increasing heating power and growing $q_\perp/q_0$, different types of behaviour can be distinguished. If ν_0 is larger than a critical value of 0.1 but does not exceed it significantly, the function f is monotonic and reveals a strong reduction of its slope for β_n in the vicinity of 1. Therefore, when $q_\perp/q_0$ exceeds a level of 0.3, the pressure gradient increases very fast. This situation of not too low plasma collisionality has been modelled in this paper. If, however, the density is sufficiently low and ν_0 is less than 0.1, $f(\beta_n, \nu_0)$ has an N-like shape. Then, a bifurcation to the state of much lower transport occurs when $q_\perp/q_0$ exceeds the critical level. This behaviour can be associated with the 'classical' L–H transition. In real plasmas the density and temperature and their gradients are interrelated, so the present analysis provides qualitative guidelines only.

6.2. Role of the radial electric field

The mechanisms responsible for the formation and sustainment of the H-mode edge barrier considered above do not include the effect from the radial electric field E_r. However, normally the shear of the drift motion induced by E_r is considered as the main cause for suppression of turbulence [1, 2]. In order to

take this channel into account, E_r is determined from the radial momentum balance for ions:

$$E_r = \frac{V_\varphi B_\vartheta - V_\vartheta B_\varphi}{c} + \frac{1}{en_i}\frac{\partial(n_i T_i)}{\partial r}, \qquad (27)$$

where $B_{\vartheta,\varphi}$ and $V_{\vartheta,\varphi}$ are the poloidal and toroidal components of the magnetic field and ion velocity, respectively. Henceforth we assume $V_\varphi = 0$ and V_ϑ given by the neo-classical theory [30], $V_\vartheta = k_{neo}(c/eB_\varphi)(\partial T_i/\partial r)$, with k_{neo} depending on the collisionality regime.

By going from the L- to H-mode conditions, the plasma density and temperature gradients become much sharper and a large sheared $\boldsymbol{E} \times \boldsymbol{B}$ rotation arises in the barrier region (see figure 3(h)). Therefore, the transport contribution of an unstable drift mode is reduced by the factor [2]

$$f = \frac{1}{1 + (\xi \cdot \omega_{\boldsymbol{E}\times\boldsymbol{B}}/\gamma_{max})^2}, \qquad (28)$$

with $\xi \approx 1$ and

$$\omega_{\boldsymbol{E}\times\boldsymbol{B}} = \frac{RB_\theta}{B}\frac{\partial}{\partial r}\left(\frac{E_r}{RB_\theta}\right). \qquad (29)$$

By applying equations (27) and (28), one gets the estimate: $\omega_{\boldsymbol{E}\times\boldsymbol{B}} \approx c_s\rho_s/(L_n L_T)$. Our computations show that this value is noticeably less than the characteristic growth rate of the edge instabilities [4], $\gamma_{max}^{edge} \approx c_s\sqrt{2/(RL_n)}$, even in the edge barrier region. Therefore, the radial electric field is not so efficient in suppressing edge instabilities as the mechanisms considered above, i.e. low collisionality and high pressure gradient.

The situation may be different for the 'core' ITG instability, for which [13] $\gamma_{max}^{ITG} \approx 0.3c_s/\sqrt{RL_T} < \gamma_{max}^{edge}$. Figure 8 shows profiles of the ion heat conductivity and temperature found under different assumptions about the mechanism for reduction of ITG-driven transport, i.e. by including separately and simultaneously the effects due to density gradient and electric field. One can see that in this case also the $\boldsymbol{E} \times \boldsymbol{B}$ rotation shear cannot sustain a pronounced barrier on its own and the density gradient works more efficiently. Our results do not exclude of course the fact that the effect from the $\boldsymbol{E} \times \boldsymbol{B}$ rotation shear can be more important under other plasma conditions.

7. Conclusions

The RITM code coupled with the transport model, which takes into account the contributions from different unstable drift modes, allows a self-consistent modelling both of L- and H-mode conditions. Computations show that the transport barrier arises when the heating power exceeds a critical level and anomalous transport induced both by 'edge' and 'core' unstable modes becomes suppressed at the plasma edge. This happens owing to decreasing collisionality and increasing gradients of the density and pressure. The width of the barrier is determined by the condition for the suppression of the ITG-mode with the density gradient and scales as the penetration depth of recycling neutrals. The scaling of the power threshold for the L–H transition with engineering parameters found by quasi-stationary RITM computations mimics well the experimental findings on JET. For the suppression of unstable modes and maintaining of the edge transport barrier, the $\boldsymbol{E} \times \boldsymbol{B}$ rotation shear is less important compared to other mechanisms considered.
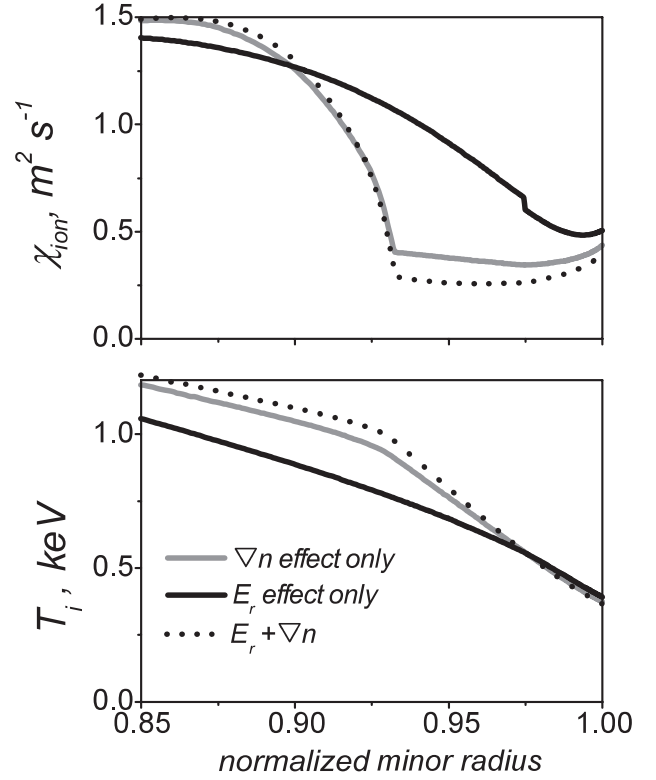

Figure 8. Ion heat conductivity and temperature computed for JET parameters under different assumptions about the mechanisms for reduction of ITG-driven transport.

References

[1] Burrell K.H. 1997 *Phys. Plasmas* **4** 1499
[2] Terry P.W. 2000 *Rev. Mod. Phys.* **72** 109
[3] Connor J.W. and Wilson H.R. 2000 *Plasma Phys. Control. Fusion* **42** R1
[4] Rogers B.N. *et al* 1998 *Phys. Rev. Lett.* **81** 4396
[5] Kerner W. *et al* 1998 *Contrib. Plasma Phys.* **38** 118
[6] Janeschitz G. *et al* 1999 *J. Nucl. Mater.* **266–269** 843
[7] Pearlstein L.D. and Berg H.L. 1969 *Phys. Rev. Lett.* **23** 220
[8] Ross W.R. and Mahajan S.M. 1978 *Phys. Rev. Lett.* **40** 324
[9] Scott B. 1990 *Phys. Rev. Lett.* **65** 3289
[10] Scott B. 1998 *Plasma Phys. Control. Fusion* **40** 823
[11] Fukuyama A. *et al* 1996 *Plasma Phys. Control. Fusion* **38** 1319
[12] Itoh S.-I. *et al* 1994 *Phys. Rev. Lett.* **72** 1200–3
[13] Weiland J. 2000 *Collective Modes in Inhomogeneous Plasma* (Bristol: Institute of Physics Publishing)
[14] Tokar M.Z. *et al* 2000 *Phys. Rev. Lett.* **84** 895
[15] Kadomtsev B.B. and Pogutse O.P. 1971 *Nucl. Fusion* **11** 67
[16] Tokar M.Z. 2004 *Phys. Rev. Lett.* **93** 239502
[17] Tokar M.Z. 1994 *Plasma Phys. Control. Fusion* **36** 1819
[18] Tokar M.Z. *et al* 1997 *Plasma Phys. Control. Fusion* **39** 569
[19] Kalupin D. *et al* 2001 *Plasma Phys. Control. Fusion* **43** 945
[20] Tokar M.Z. *et al* 2002 *Plasma Phys. Control. Fusion* **44** 1903
[21] Kalupin D. *et al* 2003 *Plasma Phys. Control. Fusion* **45** 1501
[22] Unterberg B. *et al* 2004 *Plasma Phys. Control. Fusion* **46** A241
[23] Tokar M.Z. 1993 *Plasma Phys. Control. Fusion* **35** 1119
[24] Dumortier P. *et al* 2002 *Plasma Phys. Control. Fusion* **44** 1845
[25] Nilsson J. and Weiland J. 1994 *Nucl. Fusion* **34** 803
[26] Tokar M.Z. *et al* 2005 Role of thermal instabilities and anomalous transport in threshold of detachment and multi-facetted asymmetric radiation from the edge (MARFE) *Phys. Plasmas* at press
[27] Guzdar P.N. 1993 *Phys. Fluids* B **5** 3712

[28] Horton W. 1985 *Plasma Phys. Control. Fusion* **27** 937

[29] Baker D.R and Rosenbluth M.N. 1998 *Phys. Plasmas* **5** 2936

[30] Hirshman S.P. and Sigmar D.J. 1981 *Nucl. Fusion* **21** 1079

[31] Onjun T. *et al* 2002 *Phys. Plasmas* **9** 5018

[32] JET team 2002 *Nucl. Fusion* **42** 86

[33] Wolf R. *et al* 2003 *Plasma Phys. Control. Fusion* **45** 1757

[34] Mahdavi M.A. *et al* 2002 *29th EPS Conf. on Controlled Fusion and Plasma Phys. (Montreux, 17–21 June 2002)* vol 26B, (ECA) p 2.098

[35] Hatae T *et al* 1998 *Plasma Phys. Control. Fusion* **40** 1073

[36] Snipes J.A. *et al* 2002 *Fusion Energy 2002: Proc. 19th Int. Conf. (Lyon, 2002)* (Vienna: IAEA) CD-ROM fileTERCT-P/04, http://www.iaea.org/programmes/ripc/physics/fec2002/html/fec2002.htm

[37] Andrew Y. *et al* 2003 *Plasma Phys. Control. Fusion* **46** 337

[38] ITPA H-mode Threshold Database Working Group 2004 *Proc. 20th Int. Fusion Energy Conf. (Vilamoura, 2004)* pp 3–35